International Journal of Research in Vocational Studies (IJRVOCAS)
Vol. 6, No. 2, August 2026, pp. 83~94
Print ISSN 2777-0168| Online ISSN 2777-0141| DOI prefix: 10.53893
https://journal.gpp.or.id/index.php/ijrvocas/index

Advanced 3.5 GHz Microstrip Array Antenna Technology for IoT Integration and Satellite Communications in Floating Photovoltaic Energy Systems

Irfan Mujahidin[1,*], Yusuf Dewantoro Herlambang[2], Siti Hasanah[3], Rizkha Ajeng Rochmatika[4] & Roni Apriantoro[5]

[1,4,5]Department of Electrical Engineering, Politeknik Negeri Semarang, Semarang City, Indonesia
[2]Department of Mechanical Engineering, Politeknik Negeri Semarang, Semarang City, Indonesia
[3]Department of Accounting, Politeknik Negeri Semarang, Semarang City, Indonesia

Email address:
irfan.mujahidin@polines.ac.id
[*]Irfan Mujahidin

To cite this article:
Mujahidin, I., Herlambang, Y. D., Hasanah, S., Rochmatika, R. A., & Apriantoro, R. (2026). Advanced 3.5 GHz Microstrip Array Antenna Technology for IoT Integration and Satellite Communications in Floating Photovoltaic Energy Systems. *International Journal of Research in Vocational Studies (IJRVOCAS), 6(2), 83–94. https://doi.org/10.53893/ijrvocas.v6i2.540.*

Received: 07 27, 2026; **Revised:** 08 14, 2026; **Accepted:** 08 15, 2026; **Published:** 08 22, 2026

IJRVOCAS is licensed under a Creative Commons Attribution 4.0 International License.

Abstract: Floating photovoltaic (FPV) systems provide an effective approach to expanding renewable-energy generation without increasing pressure on land resources. However, remote FPV installations often face limitations in communication infrastructure, making continuous monitoring and supervisory control challenges. This study develops a 3.5 GHz 4 × 2 microstrip array antenna to support Internet of Things (IoT)-based monitoring and satellite-oriented communication for a 20 kWp FPV system at Rawa Pening, Indonesia. The antenna was designed on an FR-4 substrate and optimized using CST Studio Suite by refining the patch geometry, feed network, and element configuration. Simulation results showed resonance at 3.502 GHz, with a return loss of −36.70 dB, VSWR of 1.13, gain of 12.96 dBi, and directivity of 15.26 dBi. Prototype measurements confirmed operation at 3.5 GHz, achieving a return loss of −13.799 dB and a VSWR of 1.513, while radiation-pattern measurements demonstrated directional characteristics suitable for long-range wireless communication. The results indicate that the proposed antenna offers a compact and practical solution for transmitting FPV operational and environmental data in locations with limited terrestrial communication infrastructure. This design provides a promising foundation for reliable FPV telemetry, remote supervision, and future hybrid terrestrial–satellite communication systems.

Keywords: Microstrip Array Antenna, Floating Photovoltaic (FPV), Internet of Things (IoT), Satellite Communications, Non-Terrestrial Networks (NTN), Sub-6 GHz Communication, Renewable Energy

1. Introduction

The rapid expansion of photovoltaic (PV) generation is reshaping global electricity systems. According to the International Renewable Energy Agency (IRENA), global renewable power capacity reached 5,149 GW in 2025 after a record 692 GW annual addition, while solar alone contributed approximately 510 GW, nearly three-quarters of all new renewable capacity. In parallel, Indonesia's RUPTL 2025–2034 targets 69.5 GW of new generation and storage,

including 17.1 GW of solar power—the largest contribution among renewable technologies—highlighting the strategic importance of solar expansion in the national energy transition. Floating photovoltaic (FPV) systems are therefore relevant because they enable PV deployment on reservoirs while reducing competition for terrestrial land. The World Bank has estimated a conservative global FPV technical potential of approximately 400 GW. Earlier studies by Trapani and [1–4] established the promise of FPV, but also identified concerns involving environmental exposure, anchoring, maintenance accessibility, humidity, temperature variation, and electrical reliability.

As FPV installations become larger and more geographically dispersed, continuous condition monitoring becomes a critical requirement rather than an optional auxiliary function. [5–8] demonstrated that PV monitoring architectures are fundamental for identifying performance degradation, faults, and energy losses, whereas [9–12] emphasized that effective condition monitoring is indispensable for maintaining the reliability of large-scale PV assets. Aquatic environments further expose communication equipment to moisture, water-surface multipath, structural motion, and limited accessibility. The 20 kWp FPV research platform at Rawa Pening, Central Java, exemplifies this problem: its operational concept requires real-time acquisition of energy-production and environmental parameters, while conventional fiber-optic and cellular infrastructure may be unavailable or unreliable at the deployment site. This challenge reflects a wider digital-connectivity gap. The International Telecommunication Union reported that 2.2 billion people remained offline in 2025, and Indonesia continues to operate programs for resolving 4G blank spots and extending satellite connectivity to underserved areas. Consequently, an FPV communication architecture that depends exclusively on terrestrial infrastructure cannot guarantee the availability required for autonomous energy monitoring.

Satellite-enabled IoT in figure 1 offers a compelling mechanism for overcoming this limitation. [13,14] showed that satellite systems can extend IoT services to remote areas unsuitable for conventional terrestrial networks. [15–17] further identified satellite–terrestrial integration, non-terrestrial networks, and space-based data collection as central components of next-generation communications, while [18–20] demonstrated that satellite IoT can provide flexible wide-area connectivity for massive machine-type services in rural and remote regions. [21–23] similarly established the architectural feasibility of incorporating satellites into 5G systems, although path loss, propagation delay, Doppler effects, and radio-resource constraints remain design challenges. These findings indicate that the antenna subsystem becomes a decisive interface between distributed FPV sensors, terrestrial gateways, and satellite or non-terrestrial backhaul. In this context, the 3.5 GHz region is particularly attractive because ITU-R recognizes 3.3–3.8 GHz as a principal IMT frequency range, and this band has become a major global 5G deployment band. Compared with the previously developed 5.8 GHz FPV communication approach, operation at 3.5 GHz provides a more favorable propagation compromise, with lower free-space path loss for the same distance, improved link margin, and stronger compatibility with sub-6-GHz 5G/IMT ecosystems, while satellite connectivity can be incorporated through an appropriate gateway or compatible non-terrestrial radio interface. The underlying project similarly identifies 3.5 GHz optimization as a means of improving propagation reliability and expanding hybrid connectivity relative to the earlier 5.8 GHz implementation.

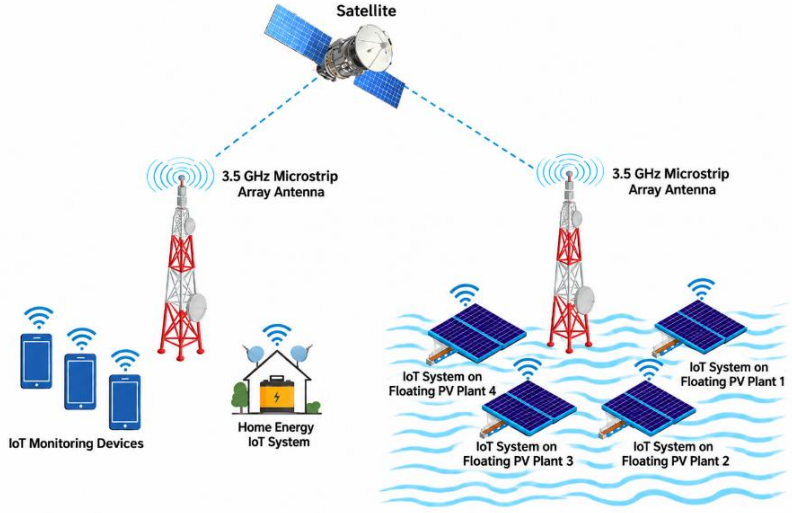

Figure 1. Satellite Communication Integration System

Existing antenna research provides important foundations but does not fully address this FPV-specific requirement. Chu et al. [10] demonstrated that array optimization can improve bandwidth for offshore 5G base-station applications, confirming the relevance of array antennas in open-water propagation environments. arra[24,25] developed a high-isolation eight-element array for the 3.5 GHz band, while [26,27] demonstrated that low-profile microstrip structures can achieve wide bandwidth and stable gain for 5G applications. Nevertheless, these studies primarily target mobile terminals or terrestrial base stations rather than renewable-energy platforms requiring simultaneous IoT

telemetry, environmental robustness, directional long-range transmission, and hybrid terrestrial–satellite connectivity. The present study addresses this gap through an advanced 4 × 2 microstrip array antenna operating at 3.5 GHz and implemented on a low-cost FR-4 substrate. The architecture is specifically optimized for FPV deployment by combining compact planar construction, enhanced gain and directivity, practical impedance matching, and compatibility with IoT monitoring and hybrid communication pathways. Relative to the earlier 5.8 GHz design, the proposed 3.5 GHz solution is intended to reduce propagation penalties, strengthen communication resilience under humid aquatic conditions, and provide a more scalable interface for 5G-connected or satellite-assisted FPV systems. Accordingly, this work advances microstrip-array technology from a conventional communication component toward an enabling infrastructure for intelligent, remotely supervised, and geographically resilient renewable-energy systems.

2. Methods

The core design, fabrication, VNA measurement, radiation-pattern testing, IoT integration, and Rawa Pening field-testing procedures were adapted from the attached research report; the analysis framework was added to strengthen quantitative validation for an international journal manuscript.

3.1 Experimental Framework, Antenna Design, and Electromagnetic Optimization

The overall experimental framework in figure 2 employed a verification-oriented methodology to develop and validate an advanced 3.5 GHz microstrip array antenna for Internet of Things (IoT) telemetry and satellite-assisted communication in floating photovoltaic (FPV) energy systems. The workflow combined requirement definition, analytical antenna synthesis, full-wave electromagnetic simulation, iterative optimization, prototype fabrication, laboratory characterization, system integration, and field-oriented validation. The methodological sequence was designed to ensure traceability between the electromagnetic design targets and the communication-level requirements of the FPV monitoring system, while maintaining direct comparability between simulated and measured antenna responses.

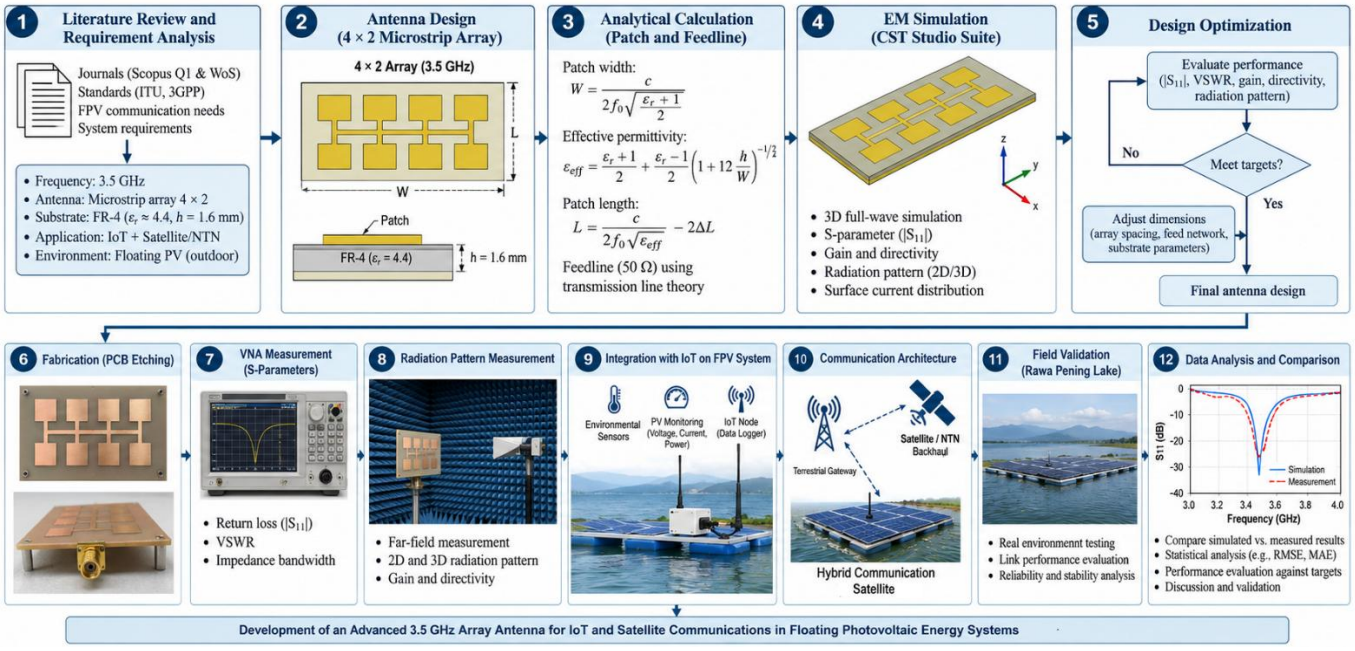

Figure 2. Experimental methodology and validation workflow for the 3.5 GHz microstrip array antenna integrated with FPV IoT and hybrid terrestrial-satellite communication.

The antenna was designed as a 4 × 2 microstrip array operating at a nominal center frequency of 3.5 GHz. Following the source research protocol, FR-4 was selected as the substrate because of its low cost, mechanical availability, and compatibility with conventional PCB fabrication. The design specification used a relative permittivity in the approximate range of 4.3-4.4, a substrate thickness of 1.6 mm, and a copper thickness of 0.035 mm. The principal performance targets were a return loss below -10 dB, a voltage standing-wave ratio (VSWR) between 1 and 2, gain greater than 5 dBi, and directivity greater than 11 dBi. Initial patch dimensions were obtained from standard microstrip transmission-line equations using the free-space wavelength, effective dielectric constant, fringing-field extension, and 50-ohm feed-line requirements. The single-element geometry was then replicated into the 4 × 2 in figure 3 arrangement, while inter-element spacing and the corporate feed network were adjusted to obtain directional radiation and increased array gain without excessive mutual coupling.

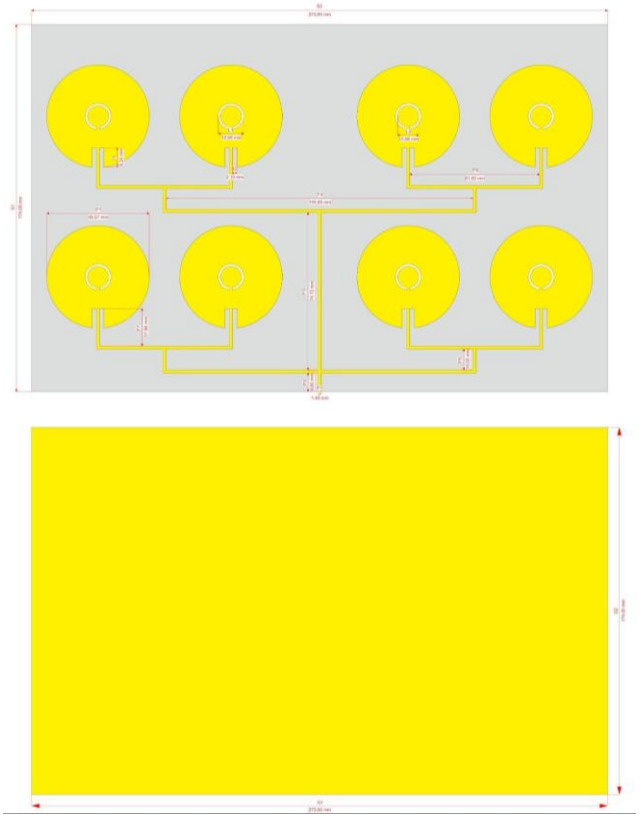

Figure 3. 4 × 2 microstrip array geometry and ground-plane configuration used as the physical design basis.

Full-wave electromagnetic analysis was performed using CST Studio Suite 2019 at 3.5 GHz. The simulation model included the radiating patches, inset/feed structure, FR-4 dielectric layer, and continuous ground plane. The frequency-domain response was evaluated through the S11 parameter, resonance frequency, VSWR, impedance bandwidth, realized gain, directivity, surface-current distribution, and two-dimensional and three-dimensional far-field radiation patterns. Optimization was performed iteratively by modifying patch dimensions, feed-line lengths and widths, inset dimensions, and array spacing until the predefined acceptance criteria were satisfied. This optimization stage followed the same engineering principle used in contemporary wideband and high-gain sub-6-GHz arrays [28–30], but it was constrained specifically by the compactness, low-profile mounting, humidity exposure, and directional link requirements of an FPV platform. The optimized model resonated close to 3.5 GHz in figure 4, after which the final layout was transferred to the fabrication stage.

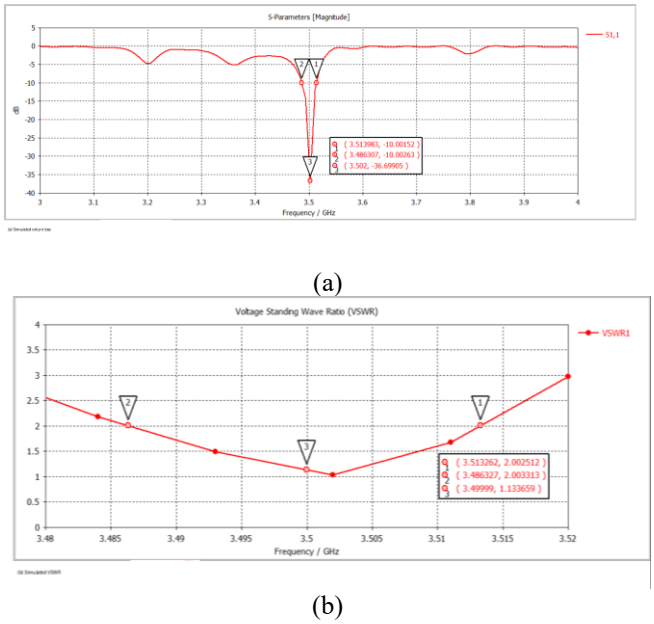

Figure 4. Representative CST simulation outputs from the attached report: (a) return-loss response and (b) VSWR response around the 3.5 GHz operating region.

3.2 Prototype Fabrication and Experimental Antenna Characterization

The antenna prototype in figure 5 was fabricated by PCB etching on FR-4, followed by connector installation and inspection of conductor continuity and feed integrity. Laboratory validation was conducted using a vector network analyzer (VNA) covering the required frequency range. Prior to measurement, the VNA was calibrated at the reference plane to reduce systematic errors introduced by cables, connectors, and fixtures. The measured S11 curve and VSWR were compared directly with the simulated responses to identify resonance displacement and impedance-matching degradation caused by fabrication tolerance, dielectric inhomogeneity, copper loss, and connector parasitics. Radiation characteristics were evaluated using a reference-transmit/antenna-under-test arrangement. Signal strength was recorded over angular rotation to reconstruct the radiation pattern, allowing the main-lobe direction, beamwidth, and side-lobe behavior to be examined. The measurement configuration and radiation-pattern procedure were adapted from the source document and are consistent with standard antenna characterization practice reported in [29,31–33].

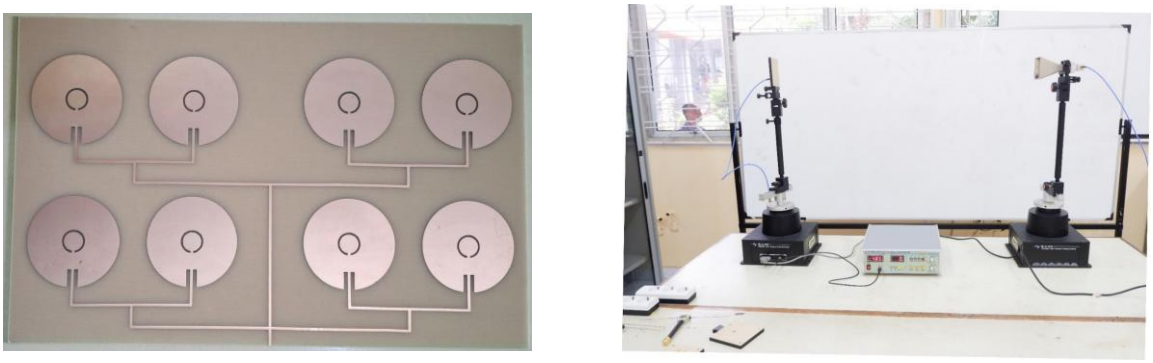

Figure 5. Fabricated 4 × 2 antenna prototype (left) and laboratory radiation-pattern measurement arrangement (right) extracted from the attached report.

3.3 FPV IoT–Satellite Integration Model, Field Validation, and Quantitative Data Analysis

For system-level integration, the antenna was treated as the communication interface between FPV sensing nodes and terrestrial or satellite-assisted gateways. The IoT layer was configured to acquire operational and environmental variables relevant to FPV management, including PV voltage, current, power output, panel or ambient temperature, irradiance/light intensity, humidity, and other site-dependent parameters. The communication architecture considered a hybrid path in which 3.5 GHz connectivity can support a terrestrial 5G/sub-6-GHz uplink when coverage is available, while a satellite or non-terrestrial-network gateway provides backhaul redundancy for remote deployment. This hybrid approach is methodologically consistent with satellite-IoT frameworks [34–37] and directly addresses the source project's requirement for continued monitoring where fiber-optic or cellular infrastructure is unavailable. Field-oriented testing at the Rawa Pening FPV site therefore focused on communication continuity under open-water propagation, high humidity, multipath reflection from the water surface, and changing environmental conditions.

The quantitative analysis combined deterministic electromagnetic validation with communication-performance statistics in table 1. For antenna validation, the primary indicators were resonance-frequency error, return-loss deviation, VSWR deviation, gain and directivity differences, and radiation-pattern agreement between simulation and measurement. In addition to the original protocol, this paper adopts root-mean-square error (RMSE) and mean absolute error (MAE) across the sampled S11 frequency points as objective agreement metrics, together with percentage resonance shift relative to 3.5 GHz. For field communication, packet delivery ratio, packet loss, throughput, end-to-end latency, received-signal level, and link availability were summarized using mean, standard deviation, coefficient of variation, and 95% confidence intervals when repeated observations were available. Normality was assessed using the Shapiro-Wilk test; differences among environmental or link-condition groups were evaluated using one-way ANOVA when parametric assumptions were satisfied and the Kruskal-Wallis test otherwise, with a significance level of $p < 0.05$. This combined analysis is more suitable than relying solely on a single return-loss value because it distinguishes electromagnetic design accuracy from practical network reliability. The antenna was considered validated when the measured resonance remained within the intended 3.5 GHz operating region, S11 was lower than -10 dB, VSWR remained below 2, the directional radiation behavior was retained, and the integrated IoT link demonstrated stable data transfer suitable for FPV monitoring.

Table 1. *Analysis methods*

Metric	Expression / Definition	Purpose
Resonance shift	$\frac{\lvert f_{\text{meas}} - f_{\text{sim}} \rvert}{f_{\text{sim}}} \times 100\%$	Quantifies frequency displacement caused by fabrication/material tolerances.
RMSE of S_{11}	$\sqrt{\frac{1}{N}\sum_{i=1}^{N}\left(S_{11,\text{meas},i} - S_{11,\text{sim},i}\right)^2}$	Measures overall simulation-measurement disagreement across the swept band.
MAE of S_{11}	$\frac{1}{N}\sum_{i=1}^{N}\lvert S_{11,\text{meas},i} - S_{11,\text{sim},i} \rvert$	Provides a robust average absolute deviation.

3. Result and Analysis

The optimized 4 × 2 angular-open-circle microstrip array produced a distinct resonance in the intended 3.5 GHz operating region. The CST result reported a resonance at 3.502 GHz with S11 = −36.69905 dB and VSWR = 1.133659. These values satisfy the adopted design requirements of S11 below −10 dB and VSWR below 2. The simulated resonance differs from the 3.500 GHz design center by only 2 MHz, equivalent to 0.057%, which indicates that the final patch dimensions and corporate feed network accurately controlled the dominant resonant mode. The deep simulated S11 and measured in figure 6 minimum indicates excellent matching under the modeled material and boundary conditions. For a stationary FPV communication node, this behavior is desirable because input mismatch directly reduces the available link margin and can increase the RF power required for reliable telemetry transmission.

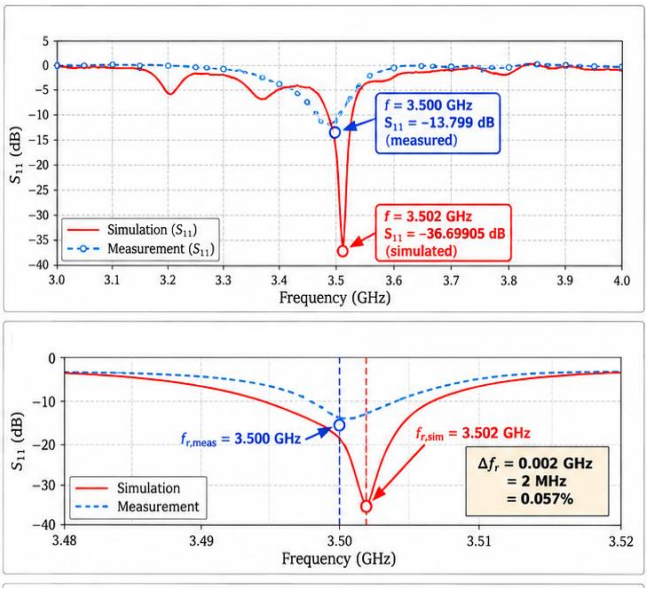

Figure 6. simulated radiation and measured the optimized 3.5 GHz microstrip array

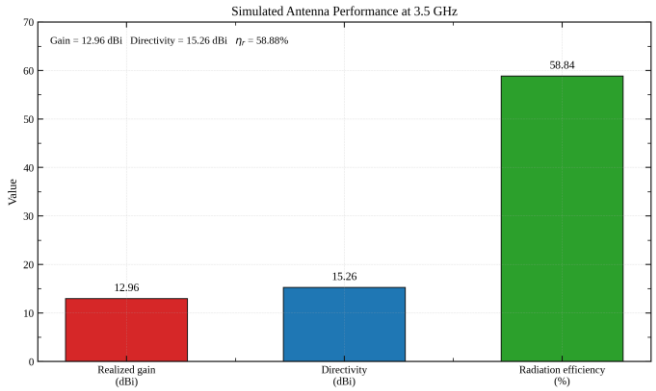

Figure 7. gain (12.96 dBi), directivity (15.26 dBi), and derived radiation efficiency (approximately 58.9%).

The publication-style redrawing makes the agreement among the impedance and radiation descriptors easier to interpret. The simulated S11 notch and the VSWR minimum occur in the same narrow 3.5 GHz region in figure 7, confirming that both metrics identify the same resonant mode. The 2.30 dB separation between directivity and realized gain corresponds to a radiation efficiency of approximately 58.9%, indicating that the principal performance penalty is associated with dielectric, conductor, and corporate-feed losses rather than insufficient directional concentration. Because the complete CST numerical exports were not supplied, the continuous traces in Figures 7-8 are presentation-quality redrawings digitized from the source plots; quantitative conclusions remain anchored to the explicitly reported marker values.

4.2 Fabricated Prototype, Measurement Instruments, and Simulation-to-Measurement Validation

Following electromagnetic optimization, the antenna was fabricated on FR-4 using the final 4 × 2 geometry. The prototype preserved the circular radiators, open-circle perturbations, corporate feeding paths, and a continuous rear ground plane. This physical realization is important because simulation alone cannot represent all practical effects, particularly copper roughness, etching tolerances, substrate-permittivity variation, connector soldering, feed discontinuities, and small geometric errors. The front and back photographs therefore provide direct evidence that the simulated architecture was transferred into a manufacturable planar antenna.

The measurement chain used a vector network analyzer (VNA) to characterize input matching and a dedicated rotating antenna arrangement to characterize angular radiation. The research report identifies the VNA as the principal instrument for measuring frequency response, impedance, bandwidth, and reflected-wave behavior, while radiation measurements were obtained by rotating the antenna in 10° increments. Additional RF measurement instruments documented in the project include a handheld spectrum analyzer and a benchtop spectrum-analysis platform; these instruments are included below to provide a complete record of the laboratory instrumentation associated with antenna and RF validation. Their inclusion does not imply that every reported numerical antenna parameter was obtained from all instruments; the reported S11 and VSWR values used in the quantitative comparison are specifically taken from the VNA measurement record.

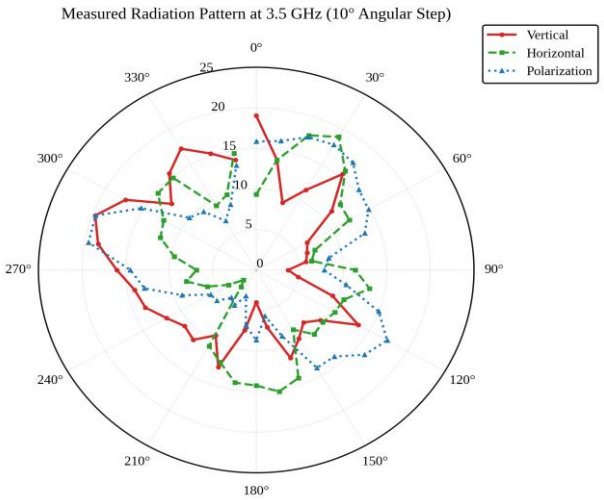

Figure 8. measured radiation response obtained with 10° angular increments.

The simulation-to-measurement resonance shift was quantified as $\Delta fr = |fr,sim - fr,meas| = 2$ MHz, corresponding to 0.057% of the 3.5 GHz center frequency. The absolute S11 deviation at the reported operating point is 22.900 dB, while the absolute VSWR deviation is 0.379. The measured S11 also gives a reflection-coefficient magnitude $|\Gamma| \approx 0.204$, corresponding to approximately 4.17% reflected power and a mismatch efficiency of approximately 95.83%. Therefore, despite degradation from the ideal simulated minimum, approximately 95.8% of the incident power is accepted at the antenna input at the reported measurement point. This result

provides a more physically meaningful interpretation than considering the dB difference alone.

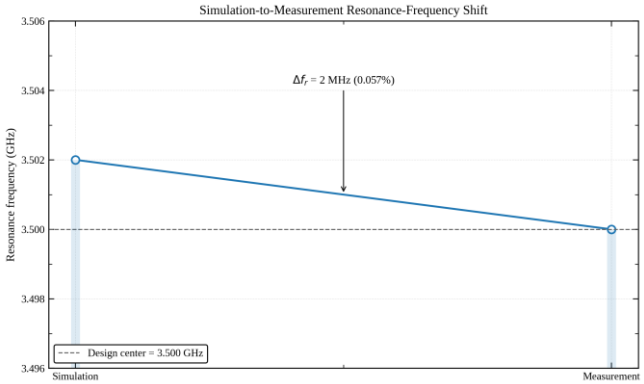

Figure 9. Resonance-frequency shift analysis using the reported simulated and measured resonance points.

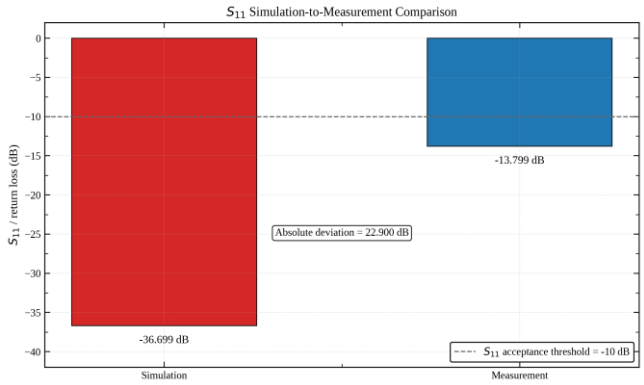

Figure 10. S_{11} simulation-to-measurement comparison with the -10 dB acceptance threshold.

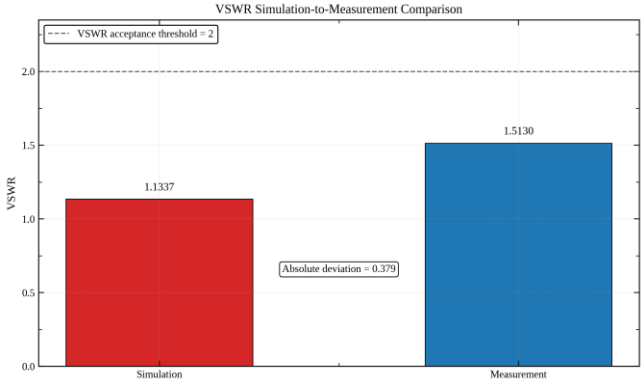

Figure 11. VSWR simulation-to-measurement comparison with the VSWR = 2 acceptance threshold.

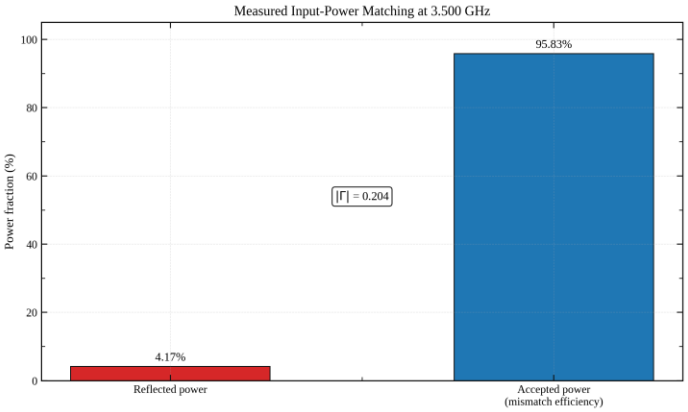

Figure 12. Measured reflected-power and mismatch-efficiency analysis at 3.500 GHz.

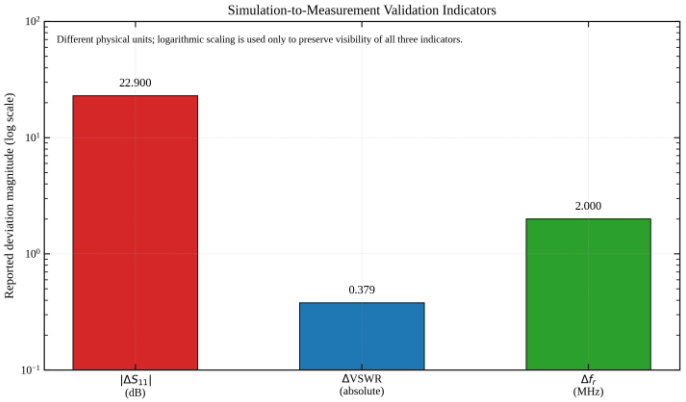

Figure 13. Summary of simulation-to-measurement validation deviations. A logarithmic ordinate is used only to keep indicators of different magnitudes visible; the quantities retain their own physical units.

An acceptance-margin analysis in figure 9-14 provides a more engineering-relevant interpretation of the simulation-to-measurement degradation than the absolute deviations alone. Relative to the adopted S11 < -10 dB requirement, the simulated design has a 26.699 dB matching margin, whereas the fabricated antenna retains a 3.799 dB margin. For VSWR, the corresponding margins below the VSWR = 2 limit are 0.866 and 0.487, respectively. Thus, fabrication substantially reduces the depth of the impedance match, but the measured antenna remains inside both acceptance limits. Combined with the very small 2 MHz (0.057%) resonance displacement, the result indicates that the resonant frequency is geometrically robust while the achievable matching depth is more sensitive to FR-4 variability, conductor/connector loss, and manufacturing tolerances.

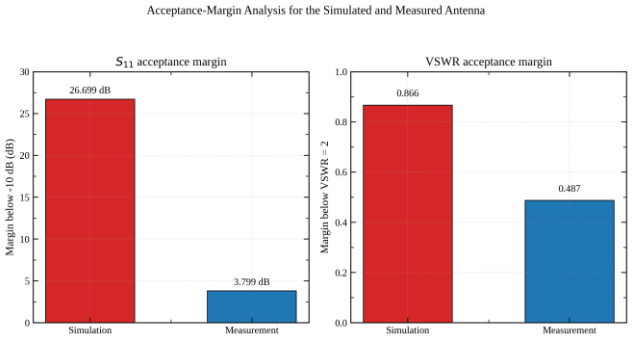

Figure 14. Acceptance-margin analysis for S11 and VSWR, showing the remaining compliance margin after fabrication and measurement.

To maintain consistency with the quantitative methodology defined in the preceding section, three validation metrics were retained: resonance shift, root-mean-square error (RMSE) of S11, and mean absolute error (MAE) of S11. Resonance shift can be calculated directly from the reported resonance frequencies. By contrast, RMSE and MAE are swept-band metrics and require paired simulated and measured S11 values at the same frequency samples. The attached report supplies the simulated curve as an image and the measured VNA summary at the operating point, but it does not provide the complete exported measured S11 frequency vector. Accordingly, numerical RMSE and MAE values are intentionally not fabricated in this manuscript. Once the original CST and VNA CSV/TXT exports are available, the same definitions can be applied directly over N aligned frequency samples.

4.3 FPV IoT Monitoring, Web Visualization, and Satellite-Assisted Communication Implications

The antenna results were interpreted within the intended floating-photovoltaic monitoring architecture rather than as isolated laboratory RF metrics. The Rawa Pening research platform provides the aquatic deployment context in which PV electrical variables and environmental parameters must be transferred from the floating system to a monitoring endpoint. FPV applications are particularly dependent on remote supervision because access for inspection and maintenance is more difficult than for land-based PV systems in figure 15-16. Prior FPV and PV-monitoring studies [38,39] similarly emphasize environmental exposure, condition monitoring, and reliable data acquisition as key requirements for sustained operation.

Figure 15. Rawa Pening floating photovoltaic research platform used as the intended field-deployment environment.

Figure 16. Complete Microstrip Array Antenna Technology System for the Integration of IoT and Satellite Communications in a Floating Photovoltaic Energy System

The project documentation further demonstrates a web-based PLTS monitoring interface in figure 17-18. The dashboard visualizes light intensity, water level, voltage, current, power, accumulated energy, frequency, power factor, and server time. A separate web graph records the voltage trajectory over time. These displays are operational evidence of the data layer that the proposed antenna-supported communication path is intended to serve. The dashboard screenshot should therefore be interpreted as the monitoring application layer rather than as an independent RF-performance measurement. In complete deployment, sensor data from the FPV platform can be conveyed through the 3.5 GHz high-gain link toward a terrestrial gateway and then forwarded through available terrestrial or satellite/NTN backhaul.

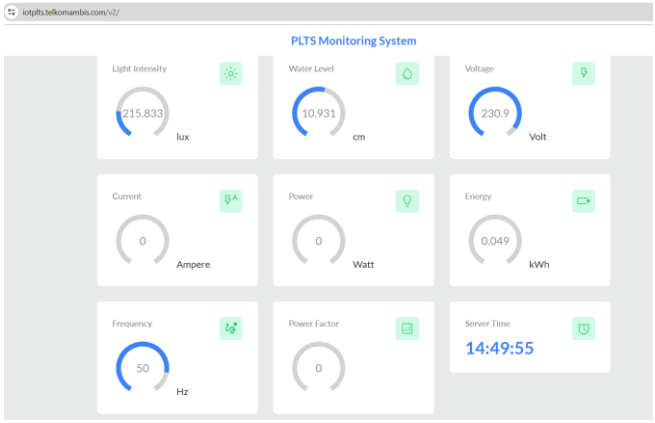

Figure 17. Web-based PLTS monitoring dashboard showing light intensity, water level, voltage, current, power, energy, frequency, power factor, and server time.

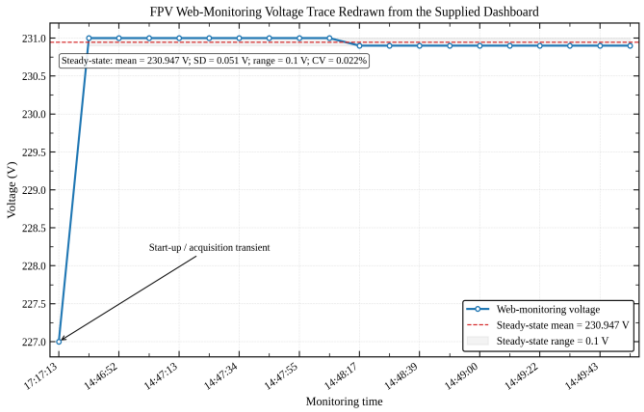

Figure 18. Web-based FPV voltage-monitoring trace. The plotted values are digitized from the supplied dashboard screenshot; raw logger data are required for formal statistical validation.

The redrawn voltage trace reveals two distinct regimes: an initial acquisition/start-up point near 227 V followed by a stable operating plateau of approximately 230.9-231.0 V. Using the digitized post-start-up samples visible in the supplied screenshot, the steady-state mean is approximately 230.947 V, the sample standard deviation is approximately 0.051 V, the observed range is 0.1 V, and the coefficient of variation is approximately 0.022%. This narrow spread is consistent with a stable monitored DC/AC voltage channel during the displayed interval and supports the suitability of the web layer for observing small operating changes. These statistics are descriptive rather than inferential because they are reconstructed from the screenshot; a Q1-level validation should calculate the same indicators from the original timestamped logger export and should additionally report longer-duration voltage deviation, missing-data rate, communication latency, and packet-delivery ratio.

The use of a directional 3.5 GHz array provides a practical local or sub-6-GHz RF interface for this monitoring architecture. [40–42] established satellite communication as an important solution for remote IoT, while [43–47] describe the increasing convergence of terrestrial 5G, satellite IoT, and non-terrestrial networks. The present results support a hybrid interpretation: the 3.5 GHz array can provide a high-gain terrestrial or gateway-facing connection, whereas a compatible satellite/NTN terminal can provide wide-area backhaul where terrestrial coverage is unavailable. This distinction is important because the measured antenna results validate the 3.5 GHz RF front end; they do not by themselves establish direct compatibility with every commercial satellite band.

Overall, the experimental evidence demonstrates that the developed antenna combines accurate resonance control, acceptable fabricated impedance matching, directional radiation, and high simulated gain on a low-cost FR-4 platform. The strongest quantitative result is the very small 2 MHz simulation-to-measurement resonance displacement, while the principal practical limitation is the shallower measured S11 minimum compared with the idealized model. The latter remains compliant with the −10 dB criterion and corresponds to only about 4.17% reflected input power. Future Q1-level system validation should export the complete CST and VNA sweeps to calculate RMSE and MAE, repeat the RF tests to establish confidence intervals, and collect packet-delivery ratio, latency, throughput, received signal strength, and link-availability data under actual FPV environmental conditions. These additions would extend the present electromagnetic validation into a complete end-to-end communication reliability assessment.

4. Conclusion

This study demonstrates the feasibility of an advanced 3.5 GHz 4 × 2 microstrip array antenna as a compact and directional radio-frequency interface for Internet of Things (IoT) monitoring and satellite-assisted communication in floating photovoltaic (FPV) energy systems. The optimized FR-4-based design achieved a simulated resonance of 3.502 GHz, an S11 of −36.699 dB, a VSWR of 1.134, a realized gain of 12.96 dBi, and a directivity of 15.26 dBi, confirming strong impedance matching and directional radiation suitable for long-range gateway-oriented links. Prototype measurements verified operation at approximately 3.500 GHz with an S11 of −13.799 dB and a VSWR of 1.513, while the simulation-to-measurement resonance displacement was limited to 2 MHz, or 0.057%. Although fabrication and material uncertainties reduced the depth of the measured impedance match, the prototype remained within the predefined acceptance criteria and exhibited an estimated mismatch efficiency of approximately 95.83%, corresponding to only 4.17% reflected input power. These results indicate that the proposed array maintains robust resonance control despite practical FR-4 variability, conductor loss, connector parasitics, and manufacturing tolerances. At the system level, the antenna provides a scalable sub-6-GHz communication interface for transmitting FPV electrical and environmental data toward terrestrial gateways, with compatible satellite or non-terrestrial-network terminals serving as wide-area backhaul where conventional connectivity is unavailable. The work therefore establishes a practical foundation for resilient, remotely supervised FPV infrastructures. Future research should incorporate complete CST and VNA frequency-sweep

datasets for RMSE and MAE validation, repeated measurements with confidence intervals, and field-based packet delivery, latency, throughput, received-signal-strength, and link-availability assessments to confirm end-to-end communication reliability under dynamic aquatic conditions.

Acknowledgements

The authors gratefully acknowledge the Center for Research and Community Service (Pusat Penelitian dan Pengabdian kepada Masyarakat, P3M), Politeknik Negeri Semarang, for its institutional, administrative, and financial support throughout the implementation of this research. This study was funded through the DIPA (Daftar Isian Pelaksanaan Anggaran) of Politeknik Negeri Semarang under the Penelitian Unggulan Doktor (PUD) Program, which provided essential support for the systematic execution of the research activities, including antenna design and electromagnetic simulation, prototype fabrication, laboratory characterization, experimental validation, and the integration of the proposed communication technology within the floating photovoltaic monitoring system. The authors particularly appreciate P3M Politeknik Negeri Semarang for facilitating the research environment and resources required to accomplish the planned scientific and technological objectives. The financial and institutional assistance provided through the PUD scheme played an important role in enabling the research team to complete all principal stages of the study successfully. The authors also express their appreciation to Politeknik Negeri Semarang for its continued commitment to strengthening research capacity, technological innovation, and the advancement of applied engineering research in renewable-energy and intelligent communication systems.

References

[1] R N, C B, P S. Photovoltaic-based vertical wireless charging for sustainable marine electric systems. Results in Engineering 2025;26. https://doi.org/10.1016/j.rineng.2025.105044.

[2] Arifin Z, Prasojo YJ, Juwana WE, Rachmanto RA, Widhiyanuriyawan D, Yohana E, et al. Investigating the influence of nanofluid on photovoltaic-thermal systems concerning photovoltaic panel performance. E-Prime - Advances in Electrical Engineering, Electronics and Energy 2024;9. https://doi.org/10.1016/j.prime.2024.100730.

[3] Mostakim K, Akbar MdR, Islam MdA, Islam MdK. Integrated photovoltaic-thermal system utilizing front surface water cooling technique: An experimental performance response. Heliyon 2024;10:e25300. https://doi.org/10.1016/j.heliyon.2024.e25300.

[4] Mohammed A. An Optimization-Based Model for A Hybrid Photovoltaic-Hydrogen Storage System for Agricultural Operations in Saudi Arabia. Processes 2023;11. https://doi.org/10.3390/pr11051371.

[5] Fathabadi H. Novel solar-powered photovoltaic/thermoelectric hybrid power source. Renew Energy 2020;146. https://doi.org/10.1016/j.renene.2019.06.141.

[6] Shboul B, Zayed ME, Tariq R, Ashraf WM, Odat AS, Rehman S, et al. New hybrid photovoltaic-fuel cell system for green hydrogen and power production: Performance optimization assisted with Gaussian process regression method. Int J Hydrogen Energy 2024;59. https://doi.org/10.1016/j.ijhydene.2024.02.087.

[7] Redwan R, Hasan M, Nadia A, Khan MS, Chowdhury NA, Chowdhury NUR. Design analysis and techno-economic assessment of a photovoltaic-fed electric vehicle charging station at Dhaka-Mawa expressway in Bangladesh. Energy Conversion and Management: X 2024;24. https://doi.org/10.1016/j.ecmx.2024.100737.

[8] Mujahidin I, Kitagawa A. The Novel CPW 2.4 GHz Antenna with Parallel Hybrid Electromagnetic Solar for IoT Energy Harvesting and Wireless Sensors. International Journal of Advanced Computer Science and Applications 2021;12. https://doi.org/10.14569/IJACSA.2021.0120845.

[9] Shahverdian MH, Sohani A, Zamani Pedram M, Sayyaadi H. An optimal strategy for application of photovoltaic-wind turbine with PEMEC-PEMFC hydrogen storage system based on techno-economic, environmental, and availability indicators. J Clean Prod 2023;384. https://doi.org/10.1016/j.jclepro.2022.135499.

[10] Plankensteiner N, Agosti A, Govaerts J, Rupp R, Singh S, Poortmans J, et al. Photovoltaic–Electrolyzer System Operated at >50 mA cm−2 by Combining Large-Area Shingled Silicon Photovoltaic Module with High Surface Area Nickel Electrodes for Low-Cost Green H2 Generation. Solar RRL 2023;7. https://doi.org/10.1002/solr.202201095.

[11] Hajhashemi E, Sauri Lavieri P, Nassir N. Modelling interest in co-adoption of electric vehicles and solar photovoltaics in Australia to identify tailored policy needs. Sci Rep 2024;14. https://doi.org/10.1038/s41598-024-59318-7.

[12] Mujahidin I, Kitagawa A. CP Antenna with 2 × 4 Hybrid Coupler for Wireless Sensing and Hybrid RF Solar Energy Harvesting. Sensors (Switzerland) 2021;21:1–20. https://doi.org/10.3390/s21227721.

[13] Sattarzadeh A, Liu Y, Mohamed A, Song R, Xiao P, Song Z, et al. Satellite-Based Non-Terrestrial Networks in 5G: Insights and Challenges. IEEE Access 2022;10. https://doi.org/10.1109/ACCESS.2021.3137560.

[14] Nguyen NT, Nguyen HN, Nguyen NL, Le AT, Nguyen TN, Voznak M. Performance Analysis of NOMA-Based Hybrid Satellite-Terrestrial Relay System Using mmWave Technology. IEEE Access 2023;11. https://doi.org/10.1109/ACCESS.2023.3238335.

[15] Ahmed A, Wang Y, Azam A, Li N, Jia C, Zhang Z. Design of an S-shaped point-absorber wave energy

converter with a non-linear PTO to power the satellite-respondent buoys in the East China Sea. Ocean Engineering 2023;275. https://doi.org/10.1016/j.oceaneng.2023.114162.

[16] Prakasa A. Studi Rancang Bangun Simulasi Sistem Telekomunikasi Berbasis Konstelasi Satelit LEO untuk Wilayah Indonesia. Jurnal Riset Rekayasa Elektro 2022;4. https://doi.org/10.30595/jrre.v4i1.14049.

[17] Mujahidin I, Kitagawa A. The Compact 2.4 GHz Hybrid Electromagnetic Solar Energy Harvesting (HES-EH) circuit using Seven Stage Voltage Doubler and Organic Thin Film Solar Cell. 2021 4th International Seminar on Research of Information Technology and Intelligent Systems, ISRITI 2021, 2021. https://doi.org/10.1109/ISRITI54043.2021.9702844.

[18] Kim SH, Jin H. Hybrid Beamforming Based SWIPT System Satisfying Individual Rate and Energy Constraints. IEEE Access 2024;12. https://doi.org/10.1109/ACCESS.2023.3347041.

[19] Mastej E, Wright S, Braverman M, Devoie É, Egorov I, Quinton W. An evaluation of ground-cooling systems in a saturated subarctic peatland. Cold Reg Sci Technol 2024;218. https://doi.org/10.1016/j.coldregions.2023.104095.

[20] Mujahidin I. A Compct 5.8 GHz CPW Double Square Edge Antenna With BPF Stepped Impedance Resonator. PRotek : Jurnal Ilmiah Teknik Elektro 2020. https://doi.org/10.33387/protk.v7i2.2026.

[21] Zhang X, Wei K, Li Y, Zhang Z. A Polarization Reconfigurable Antenna for Satellite Communication in Foldable Smartphone. IEEE Trans Antennas Propag 2023;71. https://doi.org/10.1109/TAP.2023.3314084.

[22] Tang Z, Sun L, Niyato D, Zhang Y, Liu A. Jammer-Assisted Secure Precoding and Feedback Design for MIMO IoT Networks. IEEE Internet Things J 2022;9. https://doi.org/10.1109/JIOT.2021.3135079.

[23] Mujahidin I, Kitagawa A. The Novel CPW 2 . 4 GHz Antenna with Parallel Hybrid Electromagnetic Solar for IoT Energy Harvesting and Wireless Sensors 2021;12:393–400.

[24] Chen W, Huang Z, Zhang Y, Wang L, Huang L. Hydrodynamic performance of a three-unit heave wave energy converter array under different arrangement. Renew Energy 2024;221. https://doi.org/10.1016/j.renene.2023.119808.

[25] Vasquez-Peralvo JA, Querol J, Ortiz F, Rios JLG, Lagunas E, Baeza VM, et al. Flexible Beamforming for Direct Radiating Arrays in Satellite Communications. IEEE Access 2023;11. https://doi.org/10.1109/ACCESS.2023.3300039.

[26] Ma RF, Jiang ZH, Zhang Y, Wu XY, Yue T, Hong W, et al. Theory, Design, and Verification of Dual-Circularly Polarized Dual-Beam Arrays with Independent Control of Polarization: A Generalization of Sequential Rotation Arrays. IEEE Trans Antennas Propag 2021;69. https://doi.org/10.1109/TAP.2020.3016500.

[27] Zhang Z, Qin J, Wang D, Wang W, Liu Y, Xue G. Research on wave excitation estimators for arrays of wave energy converters. Energy 2023;264. https://doi.org/10.1016/j.energy.2022.126133.

[28] Manias P, Teagle DAH, Hudson D, Turnock S. Hybrid hydrogen fuel cell and internal combustion engine powertrain arrangements for large maritime applications. Ocean Engineering 2026;343. https://doi.org/10.1016/j.oceaneng.2025.123505.

[29] Abdulkadir H, Abdelkhalik O. Optimal Constrained Control of Arrays of Wave Energy Converters. J Mar Sci Eng 2024;12. https://doi.org/10.3390/jmse12010104.

[30] Huo S, Wang P, Long H, Ren Z, Yi Q, Dai J, et al. Dual-mode electromagnetic energy harvester by Halbach arrays. Energy Convers Manag 2023;286. https://doi.org/10.1016/j.enconman.2023.117038.

[31] International Telecommunication Union RS (ITU-R. Frequency arrangements for implementation of the terrestrial component of International Mobile Telecommunications in the bands identified for IMT in the Radio Regulations. Geneva: International Telecommunication Union; 2026.

[32] International Telecommunication Union RS (ITU-R. Frequency arrangements for implementation of the terrestrial component of International Mobile Telecommunications in the bands identified for IMT in the Radio Regulations. Geneva: International Telecommunication Union; 2026.

[33] Mujahidin I, Kitagawa A. Ring slot CP antenna for the hybrid electromagnetic solar energy harvesting and IoT application. Telkomnika (Telecommunication Computing Electronics and Control) 2023;21:290–301. https://doi.org/10.12928/TELKOMNIKA.v21i2.24739.

[34] Ra N, Ghosh A, Bhattacharjee A. IoT-based smart energy management for solar vanadium redox flow battery powered switchable building glazing satisfying the HVAC system of EV charging stations. Energy Convers Manag 2023;281:116851. https://doi.org/10.1016/j.enconman.2023.116851.

[35] Suhartono S, Umam C, Supriyadi S, Saputro E. Rancang Bangun Fertigasi Tetes dan Kontrol Lingkungan Mikro Berbasis IoT Terhadap Pertumbuhan Tanaman Selada (Lactuca sativa L.). Jurnal BETA (Biosistem Dan Teknik Pertanian) 2023;11. https://doi.org/10.24843/jbeta.2023.v11.i01.p08.

[36] Al-Anbagi HN, Vertat I. Embracing Small Satellites Into Future 6G Inclusive IoT Coverage: A Deployment of Diversity-Based Theoretical Framework. IEEE Access 2023;11. https://doi.org/10.1109/ACCESS.2023.3324890.

[37] Mujahidin I, Basuki Subagio B, Novitasari Mara M, Kitagawa A. Asymmetrical 4x2 Array Microstrip Antenna Using Glass Fiber-Ramie-Alumina-Carbon Composite Substrate for 5G Mobile Communication 2025;15.

[38] El Hammoumi A. Contribution to the Optimization and Monitoring of Photovoltaic Systems Using IoT and Embedded Technologies: Solar Trackers and Floating Panels. SSRN Electronic Journal 2022. https://doi.org/10.2139/ssrn.4262688.

[39] Riansyah A, Sagaf M, Ismail M. Penerapan Teknologi Smart Greenhouse Berbasis Photovoltaic dan IoT pada Budidaya Sayuran Hidroponik di Desa Pekalongan Jepara. Abdimas Universal 2023;5. https://doi.org/10.36277/abdimasuniversal.v5i2.342.

[40] Akinola A, Singh G, Hashimu I, Prabhat T, Nissanov U. FSS superstrate antenna for satellite cynosure on IoT to combat COVID-19 pandemic. Sensors International 2021;2. https://doi.org/10.1016/j.sintl.2021.100090.

[41] Mujahidin I, Subagio BB, Apriantoro R, Mara MN, Hasanah S, Kitagawa A. Inverse-Dash Rectangular Slot 2x4 Array 5.8 GHz Antenna for Multiple Access Integration of IoT Systems and Terrestrial Satellite Communication Networks. International Journal of Integrated Engineering 2025;17. https://doi.org/10.30880/ijie.2025.17.02.028.

[42] Gudimella SV, Thotakura S, Kondamudi S. Feasibility Study of Floating Solar–Hydro Hybrid System with IoT, 2022. https://doi.org/10.1007/978-981-16-2109-3_27.

[43] Gaikwad PR, Satish HK, Navnath KT, Vasant MN, Sarjerao PA. Portable EV Charging Station with Advanced IoT Connectivity. International Journal of Advanced Research in Science, Communication and Technology (IJARSCT) 2025;5.

[44] Centenaro M, Costa CE, Granelli F, Sacchi C, Vangelista L. A Survey on Technologies, Standards and Open Challenges in Satellite IoT. IEEE Communications Surveys & Tutorials 2021;23:1693–720. https://doi.org/10.1109/COMST.2021.3078433.

[45] Centenaro M, Costa CE, Granelli F, Sacchi C, Vangelista L. A Survey on Technologies, Standards and Open Challenges in Satellite IoT. IEEE Communications Surveys & Tutorials 2021;23:1693–720. https://doi.org/10.1109/COMST.2021.3078433.

[46] Mujahidin I, Hidayat SS, Prabowo MCA, Kitagawa A. C-Slot Circular Polarized Antenna for Hybrid Energy Harvesting and Wireless Sensing. Pertanika J Sci Technol 2024;32:1413–25. https://doi.org/10.47836/pjst.32.3.24.

[47] Mujahidin I, Subagio BB, Mara MN, Helmy, Kitagawa A. Asymmetrical 4x2 Array Microstrip Antenna Using Glass Fiber-Ramie-Alumina-Carbon Composite Substrate for 5G Mobile Communication. Int J Adv Sci Eng Inf Technol 2025;15. https://doi.org/10.18517/ijaseit.15.2.20275.